Kinetics and Catalysis, Vol. 42, No. 5, 2001, pp. 703–717. Translated from Kinetika i Kataliz, Vol. 42, No. 5, 2001, pp. 773–789.

Mathematical Modeling of Nitrogen Desorption from an Iridium Surface: A Study of the Effects of Surface Structure and Subsurface Oxygen[1]

E. S. Kurkina*, N. L. Semendyaeva*, and A. I. Boronin**

** Department of Computer Science, Moscow State University, Moscow, 119899 Russia*

*** Boreskov Institute of Catalysis, Siberian Division, Russian Academy of Sciences, Novosibirsk, 630090 Russia*

Received July 20, 2000

Abstract—Thermal recombination of atomic nitrogen on iridium surfaces is studied by X-ray photoelectron spectroscopy and thermal desorption. Based on experimental data, new mathematical models are proposed and studied for nitrogen desorption from the surfaces of Ir(111), Ir(110), and iridium foil in the presence of adsorbed oxygen. The models take into account the specific features of the catalytic surface, the effect of oxygen, and the morphology of the adsorbed layer. The conditions for the appearance of an additional desorption maximum of N_2 are determined. Computational studies are carried out in the framework of point deterministic and stochastic models.

INTRODUCTION

The complete neutralization of highly toxic compounds present in the exhaust gases of internal combustion engines and industrial production is still an unsolved problem. It has been found that the conversion of nitrogen monoxide, carbon monoxide, and other toxic substances into chemically inactive compounds is most efficient when noble metals (Pt, Pd, Ir, Rh, and others) are used as catalysts [1]. The rate of chemical conversion largely depends on the chemical composition of the catalyst and its surface structure. Commercial catalysts have complex surface layer structures and provide the highest selectivity and activity in catalytic processes. Precise laboratory experiments for the mechanistic studies of surface reactions are usually carried out using well-defined single-crystal surfaces, although the faces of these single crystals have rather complex structures and contain admixtures [2]. These factors may affect experimental data and make their interpretation harder.

This work is based on experimental data obtained at the Boreskov Institute of Catalysis (Novosibirsk). We built and studied new mathematical models of atomic nitrogen recombination on Ir(111), Ir(110) and polycrystalline iridium surfaces. It was found experimentally that atomic nitrogen is formed by NO dissociation on single crystal surfaces of iridium [3] and iridium foil [4]. In the mechanistic studies of NO reduction by CO, nitrogen recombination is usually assumed to be a fast step, which is not rate-determining. More attention is usually given to the interaction of atomic oxygen with CO. However, nitrogen recombination is not a simple process. It substantially depends on the structure of the iridium surface and on the presence of atomic oxygen [5–8]. When adsorbed oxygen is present on the rough Ir(110) or polycrystalline surface, the spectra have a complex shape with two local maxima. The intensity of these maxima depends on the concentration of atomic oxygen and surface geometry [9].

Note that the interpretation of the complex spectra of the thermal desorption of NO, CO, H_2, and NH_3 molecules, as well as the products of their dissociation and interactions, from single crystal and polycrystalline surfaces is of considerable current interest [3–19]. Experimental dependences usually have several maxima and cannot be reproduced in the framework of the well-known model of the ideal adsorbed layer [20, 21]. To explain experimental thermal desorption spectra, physicochemical and mathematical models assume the existence of lateral interactions between adsorbed species [10–14], the availability of different adsorption sites on the surface [3, 4, 9, 15–19], the diffusion of atoms into the metal bulk [4, 9, 15, 17], and the geometrical or chemical nonuniformity of the surface [15, 17, 19].

In this work, the methods of mathematical modeling were used to study different effects of adsorbed oxygen on the rate of the thermal recombination of atomic nitrogen. It was shown that the appearance of additional low-temperature maximum in the thermal desorption spectra of nitrogen can be explained by the effect of subsurface atomic oxygen at the points of geometric nonuniformities and on the rough crystal faces. An alternative mechanism for the appearance of additional low-temperature maximum in the thermal desorption spectrum of N_2 is studied. This mechanism accounts for the lateral interactions of adsorbed nitrogen atoms with subsurface oxygen. It was shown that the appearance of

[1] Proceedings of the II All-Russia Workshop on Highly Organized Catalytic Systems (Moscow, June 27–30, 2000).

0023-1584/01/4205-0703$25.00

the additional low-temperature local maximum in this case could be due to the order/disorder transitions in the adsorbed layer. Finally, we studied the mutual effect of the above mechanisms on the form of the thermal desorption spectra of nitrogen. We carried out computational studies in the framework of point deterministic and stochastic models.

EXPERIMENTAL

Experiments were carried out using a VGESCA-3 electron spectrometer supplemented with several units for adsorption measurements by several *in situ* methods. XPS spectra were recorded using the AlK_α and MgK_α irradiation and an energy of analyzer transmittance of 20 eV, which corresponds to a half-width of the line Ir4$f_{7/2}$ 1.35 eV. The spectrometer was calibrated using the Au4$f_{7/2}$ and Cu2$p_{3/2}$ lines [22]. The samples with Ir(111) and Ir (110) faces and polycrystalline iridium foil were used. The surface was cleaned by the cycles of ionic etching and annealing in O_2 at 900 K and in a vacuum at temperatures higher than 1300 K. The purity of surface was controlled by the XPS spectra. Because atomic nitrogen cannot be obtained by N_2 decomposition, the layer of atomic nitrogen was formed by the atomization of nitrogen on a hot tungsten wire or using the high-frequency discharge of N_2 in the gas phase. The nitrogen coverage was determined by XPS. It was at most $[N_{ads}]^{max} \approx 4 \times 10^{18}$ atom/m^2. Adsorption was carried out at temperatures higher than 500 K. Immediately before thermal desorption, the sample was cooled to room temperature (≈300 K). Then, the sample was heated and the thermal desorption spectrum was recorded using a Q7B quadrupole mass spectrometer (VG Micromass, England).

To record the thermal desorption spectra of N_2 from the layer of coadsorbed nitrogen and oxygen, atomic nitrogen was preadsorbed on the surface, the sample was cooled to room temperature, and oxygen was dosed. Changes in the state of nitrogen depending on the oxygen coverage and adsorbate concentrations were monitored by XPS. Then, thermal desorption was registered. The rate of heating was 3–40 K/s. At this heating rate, thermal desorption spectra are the differential-type curves when the rate of desorption is proportional to the pressure of desorbing gas (the volume of a chamber was 10 l; the rate of evacuation was 100 l/s, and the sample surface area was 1 cm^2).

RESULTS

Earlier, our study of NO adsorption and the reaction of CO with NO on iridium showed that nitrogen desorbs at ~500 K. Nitric oxide dissociates before nitrogen recombination [7, 9, 23]. However, when studying the adsorbed layer consisting solely of atomic nitrogen species obtained by N_2 dissociation, we found a higher thermal stability of N_{ads} independently of the structure of iridium surface.

Figure 1 shows that the adsorbed layer of atomic nitrogen on the Ir(111) surface is thermally stable at 600 K, although additional adsorption of oxygen at 600 K or heating of the layer of co-adsorbed nitrogen and oxygen to 600 K results in the complete removal of atomic nitrogen from the surface. This effect of coadsorbed oxygen on nitrogen on Ir(111) is not instantaneous, and the kinetics of nitrogen substitution by oxygen at, say, 470 K is recorded for 30–45 min. However, in the case of the Ir(110) face or polycrystalline surface, the effect of oxygen on nitrogen is much stronger. Figure 2a shows the X-ray photoelectron N1*s* spectra and thermal desorption spectra of N_2 (Fig. 2b) from coadsorbed N_{ads} and O_{ads} on the polycrystalline surface of iridium. The N1*s* spectra show that the state of atomic nitrogen does not change when oxygen is added, although an additional low-temperature peak appears in the spectra of N_2 thermal desorption. The intensity of this peak increases with an increase in the surface concentration of atomic oxygen (Fig. 2b, spectra *2–4*). Thus, data shown in Fig. 2a suggest that at an adsorption temperature of 300 K, adsorbed oxygen does not affect the state of preadsorbed N_{ads}. Nevertheless, the thermal desorption spectrum changes drastically if coadsorbed oxygen is present. A change in the thermal desorption spectrum is due to changes in the properties of the adsorbed layer on the iridium surface under the action of oxygen when the sample is heated.

Note that the low-temperature desorption of nitrogen occurs at 500–600 K. Therefore, the modification of the surface by oxygen should occur in the same temperature range. Indeed, the XPS data for the polycrystalline surface (Fig. 3) show that when the adsorbed layer of oxygen is heated, it changes in the integral intensity and the half-width of the O1*s* begin at 300–400 K. That is, the state of oxygen changes and these changes discontinue at 700–800 K. Using a combination of XPS and *in situ* thermal desorption, we found that changes in the state of oxygen and the modification of the iridium surface occur due to the transition of oxygen into the metal bulk. Thus, Fig. 4a shows the O1*s* spectra recorded after adsorption at 400 K and after heating iridium to 700 K. Comparison of the spectra shows that, when the layer of adsorbed oxygen is heated, the peak area decreases by 20–25%. This decrease in the integral intensity of the peak is not associated with a decrease in the number of atoms on iridium because the curves of the temperature-programmed reaction $O_{ads} + CO_{ads}$ (TDS-CO_2) shown in Fig. 4b give the same peak areas for both adlayers of oxygen. These data unambiguously point to the fact that a decrease in the integral intensity of the O1*s* peak is due to the diffusion of oxygen into the bulk of iridium and the shielding of electron emission from oxygen atoms. Figure 3a shows well that, after the annealing of a saturated oxygen layer, the structure of the O1*s* peak changes. When decomposing this peak, we see that it splits into two components cor-

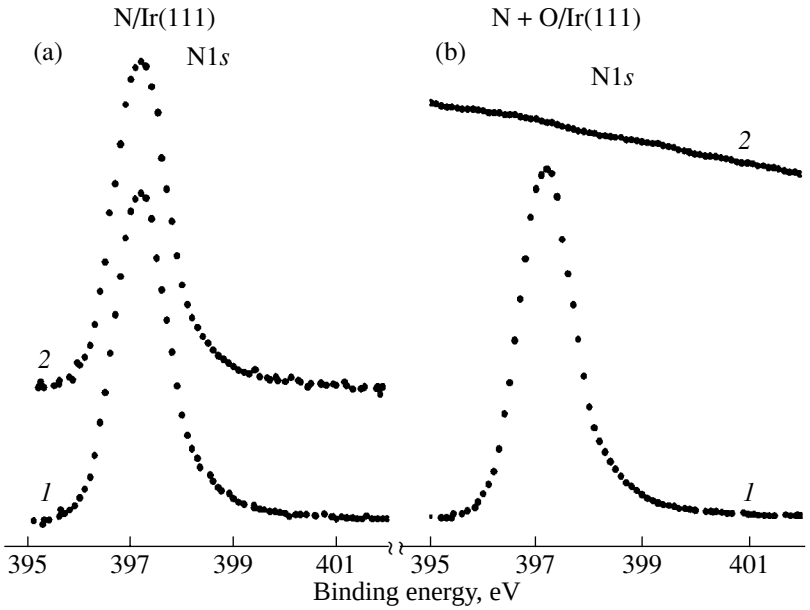

Fig. 1. XPS spectra N1*s* obtained upon the adsorption of atomic nitrogen on the Ir(111) surface (*1*) at 300 K and (*2*) after heating the crystal to 600 K (a) in a vacuum and in (b) a flow of oxygen.

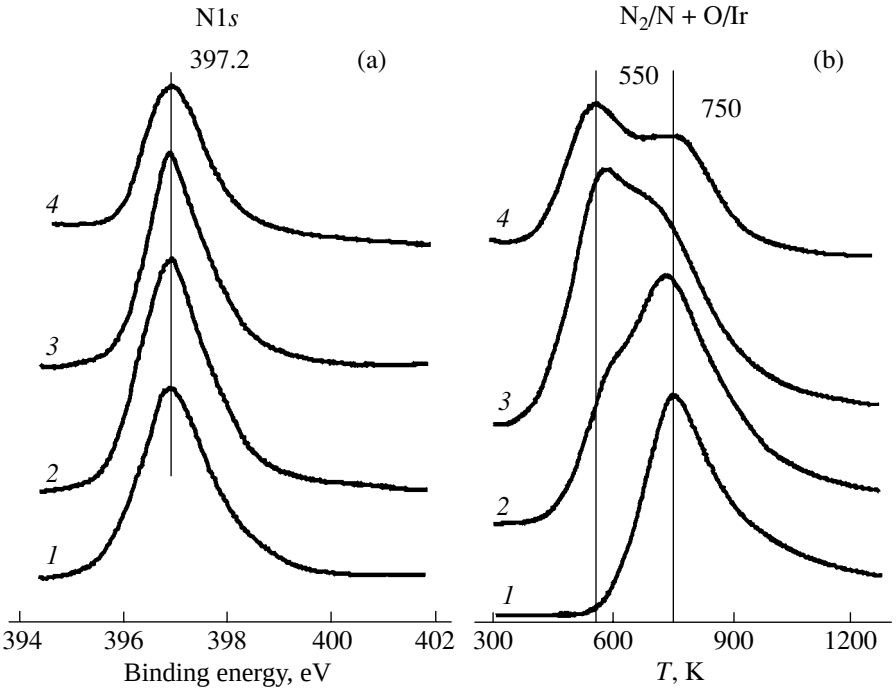

Fig. 2. (a) XPS spectra N1*s* obtained upon (*1*) the adsorption of atomic nitrogen and (*2–4*) additional adsorption of oxygen; (b) thermal desorption spectra of N_2 from (*1*) the N_{ads} layer and (*2–4*) N_{ads} + O_{ads} layer: (*1*) $[N_{ads}] = 3.0 \times 10^{14}$ atom/cm^2 and $[O_{ads}] = 0$; (*2*) $[N_{ads}] = 3.0 \times 10^{14}$ atom/cm^2 and $[O_{ads}] = 2.5 \times 10^{14}$ atom/cm^2; (*3*) $[N_{ads}] = 3.0 \times 10^{14}$ atom/cm^2 and $[O_{ads}] = 3.5 \times 10^{14}$ atom/cm^2; and (*4*) $[N_{ads}] = 2.0 \times 10^{14}$ atom/cm^2 and $[O_{ads}] = 7.0 \times 10^{14}$ atom/cm^2;

responding to two types of oxygen: subsurface and surface oxygen atoms. The diffusion of oxygen into the bulk occurs at the defect sites because subsurface oxygen is not formed on the Ir(111) surface and the effect of oxygen on nitrogen is less pronounced.

Generalized Physicochemical Model

Based on experimental data, we propose the following physicochemical model for the thermal recombination of nitrogen on the iridium surface, which seems to be the most adequate for the experimental data.

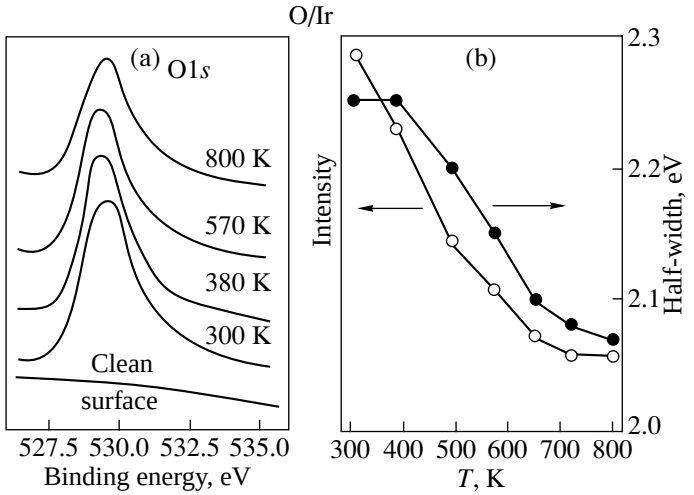

Fig. 3. (a) XPS spectra O1*s* obtained after adsorption of oxygen on iridium foil at 300 K and after stepwise heating of foil (these spectra were recorded *in situ*); (b) dependence of the half-width and the integral intensity of the line O1*s* on temperature.

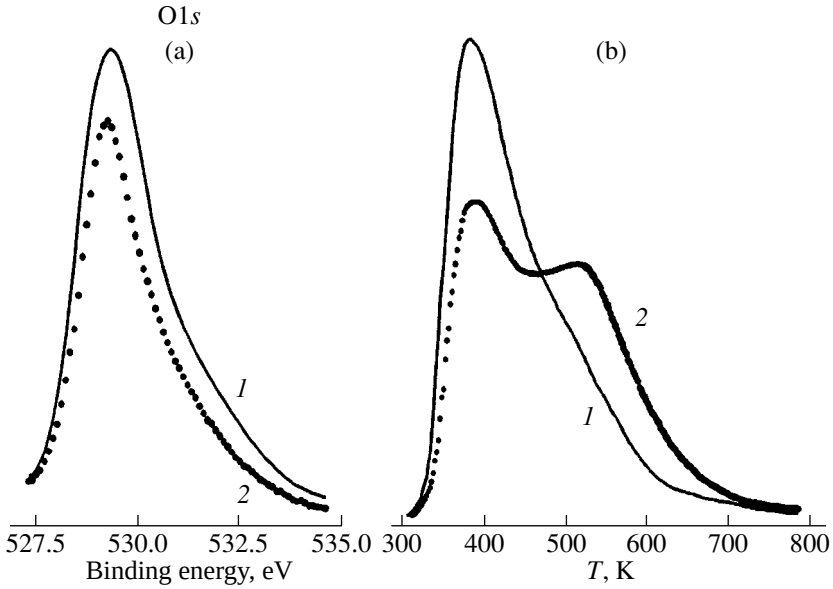

Fig. 4. (a) XPS spectra O1*s* obtained after adsorption of O_2 (*1*) at 300 K and (*2*) after further heating to 700 K, $[O_{ads}] = 5 \times 10^{18}$ atom/m^2; (b) thermal desorption spectra of CO_2 that characterize the corresponding layers of oxygen.

Because the iridium foil was not annealed and recrystallized at high temperatures (>2000 K), its surface consists of several small microcrystallites. As follows from the adsorption-kinetic behavior of the iridium foil surface and from the data of electron spectroscopy, the surface contains boundary oxygen atoms and various defects (steps, breaks, kinks, etc.) in high concentrations. According to our estimates, the number of defect iridium atoms may reach 10–20% of the total amount of surface atoms.

On the rough Ir(110) face and on the defects of the iridium foil, adsorbed atomic oxygen may transfer to the bulk and modify the properties of the nearest neighbors of adsorption sites. When atomic nitrogen is adsorbed on nonmodified sites (denoted by superscript I), it desorbs at high temperatures independently of the presence of coadsorbed oxygen. The binding of nitrogen localized on modified centers (II) weakens, and N_2 recombination and desorption occur at a low temperature. Thus, the model accounts for the two types of adsorbed atomic nitrogen: the more active $(N)^{II}$ and the less active $(N)^{I}$. The processes of nitrogen diffusion along the surface that result in transitions between these two forms of oxygen are also considered.

The kinetic scheme of the low-temperature recombination of atomic nitrogen from the adsorbed layer in the presence of atomic oxygen on the surface and subsurface oxygen consists of seven elementary steps: associative desorption of N_2 from nonmodified, modified, and mixed adsorption sites

$$(N)^{I} + (N)^{I} \longrightarrow (*)^{I} + (*)^{I} + (N_2)\uparrow \quad (k_1), \qquad \text{(I)}$$

$$(N)^{II} + (N)^{II} \longrightarrow (*)^{II} + (*)^{II} + (N_2)\uparrow \quad (k_2), \qquad \text{(II)}$$

$$(N)^{I} + (N)^{II} \longrightarrow (*)^{I} + (*)^{II} + (N_2)\uparrow \quad (k_3), \qquad \text{(III)}$$

transition of one nitrogen form into another

$$(N)^{I} + (*)^{II} \rightleftharpoons (*)^{I} + (N)^{II} \quad (k_{4+}, k_{4-}), \qquad \text{(IV)}$$

and migration of adsorbed species over energetically equivalent sites

$$(N)^{I} + (*)^{I} \rightleftharpoons (*)^{I} + (N)^{I} \quad (k_5), \qquad \text{(V)}$$

$$(O)^{I} + (*)^{I} \rightleftharpoons (*)^{I} + (O)^{I} \quad (k_6), \qquad \text{(VI)}$$

$$(N)^{II} + (*)^{II} \rightleftharpoons (*)^{II} + (N)^{II} \quad (k_7). \qquad \text{(VII)}$$

Here, $(*)^{I}$ and $(*)^{II}$ are free adsorption sites, $(N_2)\uparrow$ is the molecule in the gas phase, k_i are the rate constants of elementary steps. We assume that the surface oxygen is only adsorbed on nonmodified sites; it does not desorb or react with nitrogen. We also assume that the formation of subsurface oxygen is completed before the thermal desorption experiment

System of Mathematical Models

Some models of catalyst surface. Let us consider the models for Ir(111), Ir(110), and iridium foil surfaces.

The ideal (111) and (110) faces of an iridium single crystal are represented by a lattice of equivalent nodes with triangular L_{tr} and rectangular L_{rec} elementary cells (Fig. 5a). The nodes of lattice can be either vacant or occupied by adsorbed oxygen or nitrogen atoms. Subsurface oxygen is not formed on the close-packed Ir(111) face. Therefore, the kinetic scheme of N_2 thermal desorption consists of three elementary steps: the associative desorption of nitrogen (I) and migration of adsorbed species along the surface (V) and (VI). On the rough Ir(110) face, surface oxygen can migrate beneath the surface and the kinetic scheme of atomic nitrogen recombination involves all the seven steps. To describe the surface of iridium foil, we consider geometric nonuniformities (defects). Let us describe the surface consisting of terraces ((111) microfacets) and parallel monatomic steps (Fig. 5b). The distribution of active sites belonging to terraces and steps (or defects) is set by the lattice $L^{*}_{tr}(z)$, where $z > 0$ is the fraction of active sites on defects. The elementary cell of the lattice contains n nodes of one row of which $(n-1)$ nodes belong to a terrace and one node belongs to a defect; $z = 1/n$. Each node of the lattice belongs to either terrace or a step. For $z = 0.1$–0.2, we obtain the model of the iridium foil surface. If the ratio between the number of active sites on steps and terraces is low ($z < 0.01$), this model can be used for the more detailed description of the Ir(111) face.

If we consider another regular distribution of defects different from that shown in Fig. 5b, we can obtain new classes of models of geometrically nonuniform surfaces. In this work, we consider a chain-armor model shown in Fig. 5c in addition to a monatomic-step model. The elementary cell of the chain-armor lattice $L^{**}_{tr}(z)$ is a parallelogram covering $n^2 = nn$ nodes of which $2n-1$ nodes are at the steps and the rest $(n-1)^2$ nodes belong to a terrace.

In further developments below, we consider that surface oxygen is randomly distributed over the Ir(110) surface. On the iridium foil, the formation of subsurface oxygen occurs at the points of structural defects.

The fundamental kinetic equation. The model of multicomponent two-dimensional lattice gas and the assumption of the Markov evolution of the system form the basis for mathematical description. A finite fragment of the lattice containing N nodes with periodic boundary conditions is considered. The evolution of probabilities of the fragment state in the Markov approximation is described by the fundamental kinetic equation (FKE) [24]

$$dP_{\vec{S}}/dt = \sum_{\vec{S}'} [P_{\vec{S}'}\lambda(\vec{S}' \longrightarrow \vec{S}) - P_{\vec{S}}\lambda(\vec{S} \longrightarrow \vec{S}')] \qquad (1)$$

with the initial conditions $P_{\vec{S}}(t^0) = P^0_{\vec{S}}$. Here, $\vec{S}$ is the state of the lattice fragment at the moment t determined by the numbers s_i of covering all the active sites of the fragment, $i = 1, \ldots, N$, $s_i \in \{(*)^{I}, (N)^{I}, (O)^{I}\}$ in the case of the surface without subsurface oxygen or $s_i \in \{(*)^{I}, (N)^{I}, (O)^{I}, (*)^{II}, (N)^{II}\}$ in the case of the surface partly modified by subsurface oxygen; $P_{\vec{S}}(t)$ is the unconditional probability of the state $\vec{S}$ at the moment t; $\lambda(\vec{S}' \longrightarrow \vec{S}, t)$ is the intensity of the system transition from the state $\vec{S}'$ to the state $\vec{S}$ at the moment t.

The intensity of transition is determined by the rates of possible surface processes that transform one state of the fragment into another. It depends on the current state of the lattice fragment. In this work, we consider only two-node processes occurring on nearest neighbors. Their rates are calculated according to the transition state theory [25] with an account of lateral inter-

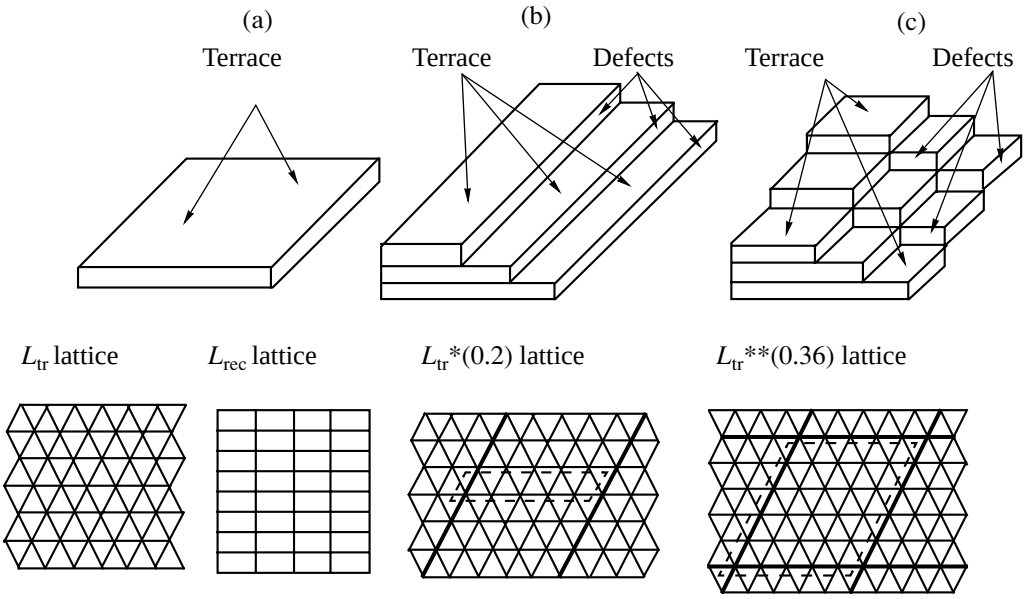

Fig. 5. Models of the catalyst surface: (a) ideal faces of Ir(111) L_{tr} and Ir(110) L_{rec}; (b, c) schematic representation of geometrically nonuniform surfaces consisting of terraces and steps and examples of their mathematical models L_{tr}^{*} (0.2) and L_{tr}^{**} (0.36).

actions in the adsorbed layer using the formulas of the form

$$k_{ij,\alpha}(t) = \delta_{ij}(t, a, b)k_\alpha I_{ij,\alpha}(t),$$
$$k_\alpha = k_\alpha^0 \exp(-\beta E_\alpha). \quad (2)$$

Here, α is the number of the elementary step, $\alpha \in \{1, \ldots, 7\}$; $i, j \in \{1, \ldots, N\}$ are the numbers of the nearest nodes in the lattice; $\delta_{ij}(t, a, b) = P(s_i = a, s_j = b) + P(s_i = b, s_j = a/a \neq b)$; a and b are the reactants in the elementary step; k_α^0 is the preexponential factor; $\beta = 1/(RT)$; R is the universal gas constant; $T(t)$ is the surface temperature; E_α is the activation energy of the elementary process at a low coverage; $I_{ij,\alpha}(t)$ is a factor that takes into account the lateral interactions of adsorbed species [12, 13].

Stochastic description. Solving the FKE system (1) straightforwardly is difficult because of its high dimensionality. For the approximate description of the dynamics of the lattice system, we can use the stochastic or deterministic methods. In the former case, separate realizations of the stochastic Markov process are constructed. In this work, to determine the phase trajectories of the lattice system in the space of states, we used the imitation algorithm with a variable time step [25]. This algorithm consists of four main stages: (1) the choice of the initial state; (2) the determination of the moment when the system terminates the current state; (3) the determination of the event; and (4) the completion of event and transfer to the second stage. The imitation of surface processes enables finding exact correlations in the arrangement of adsorbed species. It is known that the spatial distribution of species may substantially affect the dynamics of the reactive system [12]. Possible reasons for the appearance of correlations in the arrangement of adsorbed species on active sites can be lateral interactions and geometrical defects of the surface. In this work, we studied the role of each of these factors. The values of rate constants and the parameters of lateral interactions are listed in Tables 1 and 2.

Deterministic description. Cluster approximations of the FKE [26, 27] form the basis for describing the evolution of the lattice system. The simplest point model is the model of an ideal adsorbate layer, which assumes the absence of lateral interactions in the adsorbed layer and the uniform distribution of species over equivalent adsorption sites. In the framework of the ideal model, on the geometrically uniform Ir(111) and Ir(110) surfaces (Fig. 5a), the associative thermal desorption from the two-component layer (steps (I), (V), and (VI)) is described by solving the Kochi problem for one ordinary differential equation of the form

$$d\theta_N^I/dt = -\xi_1 k_1 (\theta_N^I)^2 \quad (3)$$

with the initial condition $\theta_N^I(t^0)$. Here, θ_N^I is the concentration of atomic nitrogen, $0 \le \theta_N^I(t) \le 1$; ξ_1 is a parameter equal to the number of nodes in the first coordination sphere of each node; for the lattice L_{tr}, $\xi_1 = 6$; for the lattice L_{rec}, $\xi_1 = 2$; k_1 is the rate constant of nitrogen molecule desorption (step (I)). It is well known that the solution to problem (3) has a single

Table 1. Parameters of the rates of elementary steps

Parameter	Number of step α							
	1	**2**	**3**	**4+**	**4–**	5	6	7
k_α^0, s^{-1}	$\mathbf{1.7 \times 10^9}$	$\mathbf{2 \times 10^{11}}$	$\mathbf{10^{11}}$	**25**	**25**	10^4	10^4	10^4
E_α, kcal/mol	**32**	**28**	**28**	**7**	**6**	7	7	7

Note: The values of parameters of the rates of surface processes used in deterministic models are shown in boldface.

maximum, and that its position depends on the initial conditions and the heating rate [21].

Let us consider the monatomic-step model (Fig. 5b). We divide the set of adsorption sites into two nonoverlapping subsets $L_{tr}^*(z) = L_t \cup L_z$, where L_t are nodes at terraces and L_z are nodes at structural defects. Then, we assume that all active sites at defects are affected by subsurface oxygen. Suppose that the adsorbed layer is ideal for each of the subsets. The steps of desorption from defects (II), mixed sites (III), and the steps of nitrogen exchange between terraces and defects (IV) are taken into consideration. With these assumptions, a change in the state of the adsorbed layer on the geometrically nonuniform surface of the monatomic-step type is described by two equations

$$\begin{aligned} d\theta_N^I/dt &= -\zeta_1 k_1 (\theta_N^I)^2 - \zeta_3 k_3 \theta_N^I \theta_N^{II} \\ &+ \zeta_3[-k_{4+} + \theta_N^I(z - \theta_N^{II}) + k_{4-}\theta_N^{II}(1 - z - \theta_N^I - \theta_O^I)], \\ d\theta_N^{II}/dt &= -\zeta_2 k_2 (\theta_N^{II})^2 - \zeta_3 k_3 \theta_N^I \theta_N^{II} \\ &+ \zeta_3[k_{4+} + \theta_N^I(z - \theta_N^{II}) - k_{4-}\theta_N^{II}(1 - z - \theta_N^I - \theta_O^I)]. \end{aligned} \quad (4)$$

Here, θ_N^I and θ_N^{II} are the concentrations of atomic nitrogen on terraces (or nonmodified sites) and defects (modified sites); θ_O^I is the concentration of atomic oxygen on terraces, $0 \le \theta_N^I(t) + \theta_N^{II}(t) + \theta_O^I \le 1$, z is the fraction of active sites belonging to defects, $0 < z \le 0.25$; that is, $n \ge 4$; and $0 \le \theta_N^{II}(t) \le z$; ζ_1, ζ_2, and ζ_3 are the parameters reflecting surface geometry:

$$\zeta_1 = (6 - 10z)/(1 - z)^2, \quad \zeta_2 = 2/z, \quad \zeta_3 = 4/(1 - z); \quad (5)$$

k_2 and k_3 are the rate constants of desorption from defect and mixed sites and k_{4+} and k_{4-} are the rate constants of nitrogen species exchange between terraces and defects. Note that in the cited range of z, parameters ζ_1 and ζ_2 are insensitive to the fraction of active sites at defects and change from ≈6.02 (4.04) at $z = 0.01$ to ≈6.22 (5.33) at $z = 0.25$. Parameter ζ_2 is more sensitive to z and changes from 200 at $z = 0.01$ to 8 at $z = 0.25$.

Equations (4) describe the associative desorption of nitrogen from terraces $R_{I,I} = \zeta_1 k_1 (\theta_N^I)^2$, defects with subsurface oxygen $R_{II,II} = \zeta_2 k_2 (\theta_N^{II})^2$, and mixed sites $R_{I,II} = \zeta_3 k_3 \theta_N^I \theta_N^{II}$, as well as the transition of nitrogen atoms from terraces to defects $R_{I \to II} = \zeta_3 k_{4+} \theta_N^I (z - \theta_N^{II})$ and back $R_{II \to I} = \zeta_3 k_{4-} \theta_N^{II} (1 - z - \theta_N^I - \theta_O^I)$. The system of FKE (4) is supplemented by the initial conditions $\theta_N^I(t^0)$, $\theta_N^{II}(t^0)$, and $\theta_O^I(t^0)$.

According to experimental data, the overall surface concentration of atomic nitrogen at the initial moment $\theta_N(t^0) = \theta_N^I(t^0) + \theta_N^{II}(t^0)$ is no greater than 0.20–0.25. Suppose that before the beginning of a thermal desorption experiment, nitrogen atoms are uniformly distributed over the surface: $\theta_N^I(t^0) = \theta_N(t^0)(1 - z)$, $\theta_N^{II}(t^0) = \theta_N(t^0)z$, and $\theta_N(t^0) = 0.25$. Let us set some values of the concentration of atomic oxygen on terraces (for instance, $\theta_O^I(t^0) = 0.2$), the initial temperature of the surface ($T^0 = 300$ K), and the heating rate ($b = 30$ K/s).

The values of desorption parameters (steps (I)–(III)) are borrowed from the experiment. The values of other constants were chosen to achieve the best qualitative fit of experimental and calculated thermal desorption spectra at different values of z.

Along with the monatomic-step model of the surface, we studied the chain-armor model (Fig. 5c). This

Table 2. Parameters of lateral interactions in the adsorbed layer (kcal/mol)

Number of variant	ε_{NN}^1	ε_{NO}^1	ε_{OO}^1	ε_{NN}^2	ε_{NO}^2	ε_{OO}^2
1	–1.6	–1.6	–1.6	0.8	0.8	0.8
2	–1.6	–	–	0.8	–	–
3	–1.6	–	–1.6	0.8	–	0.8

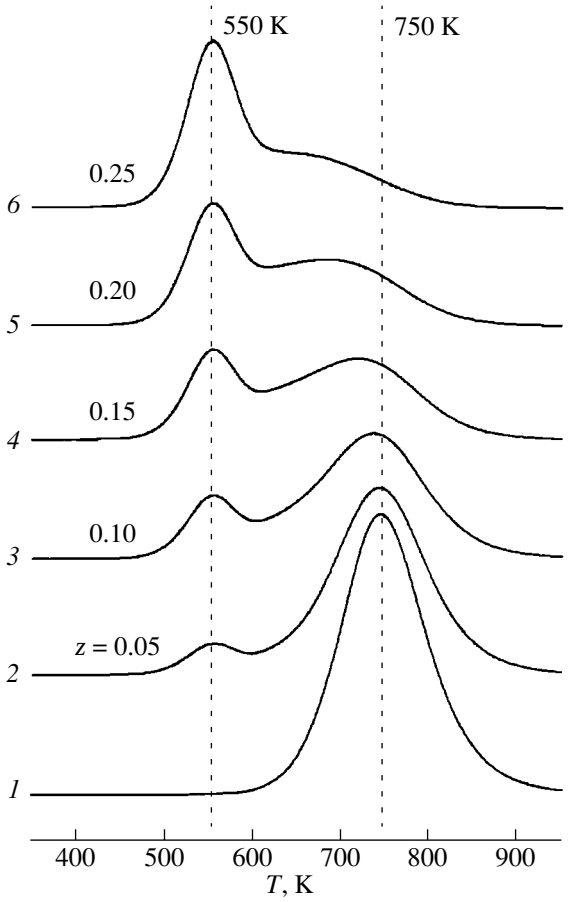

Fig. 6. Thermal desorption spectra of calculated using deterministic models: (*1*) ideal adsorbed layer, (*3*) geometrically nonuniform Ir(111) surface, (*2*–*6*) monatomic-step model (*4*)–(*5*) at different values of *z*.

model is characterized by a more complicated boundary between separate (111) microfacets and, therefore, provides a more adequate description of the polycrystalline surface. At $n \geq 4$, the fraction of defects is at most ≈44% (for $n = 4$ $z = (2n - 1)/n^2 = 7/16$ (see above). The problem of nitrogen thermal desorption for the chain-armor model is stated in an analogous way. The system of equations (4) that describes changes in the surface concentrations of nitrogen on terraces and defects for this model differs from system (4)–(5) in the form of the functional dependences of ζ_1, ζ_2, and ζ_3 on the fraction of defects:

$$\zeta_1 = [16(1-z) - 12(1-z)^{1/2} + 2]/(1-z)^2,$$

$$\zeta_2 = [4(1-z) - 12(1-z)^{1/2} + 8]/z^2, \qquad (6)$$

$$\zeta_3 = [-10(1-z) + 12(1-z)^{1/2} - 2]/z/(1-z).$$

At $z \leq 0.01$, the values of parameters ζ_1, ζ_2, and ζ_3 for the monatomic-step and chain-armor models differ by at most 1%, whereas at $z = 0.25$ the values of parameters ζ_1 and ζ_3 calculated by formula (6) are greater than the corresponding parameters of system (5) by 3 and 22%, respectively. In contrast, the value of ζ_2 for the chain-armor model is only 89% that for the monatomic-step model. Thus, we may expect that for the same values of rate parameters, the two models of geometrically nonuniform surface would give close results for low *z*. Insignificantly small quantitative changes can be expected in the case of high *z*.

Results of Mathematical Modeling

Deterministic model. Problems (4)–(6) were solved numerically using the Gear method [28]. The main goal of the study was to find conditions under which the above models qualitatively describe experimental data. This task is reducible to choosing the rate constants of desorption from the mixed sites and the rate constants for nitrogen exchange between terraces and defects.

Our studies showed that (a) it is possible to adequately describe experimental data within the framework of the proposed models of geometrically nonuniform surfaces (4)–(6), and (b) an important factor for the description of thermal desorption spectra is the assumption that the rate of nitrogen atom exchange between modified and nonmodified adsorption sites is low.

The monatomic-step model (4), (5). Figure 6 shows the thermal desorption spectra of N_2 for different concentrations of active sites on defects with subsurface oxygen $z \neq 0$ (spectra *2*–*6*) and the spectrum calculated according to ideal model (3) for $\xi_1 = 6$ (spectrum *1*). In the presence of oxygen under the surface of monatomic steps, TDS spectra have two maxima at $T_1 \approx 550$–560 K and $T_2 \approx 740$–750 K. The intensity of the low-temperature maximum increases with an increase in the concentration of subsurface oxygen *z*. This feature of thermal desorption spectra correspond to the data of real experiment.

Figure 7a shows the structure of thermal desorption spectra at $z = 0.15$. Nitrogen desorption from defects $R_{II, II}$ at low temperatures (below 600 K) and from terraces $R_{I, I}$ at higher temperatures contribute noticeably to the overall rate of desorption *R*. The desorption of nitrogen from mixed sites is rather intensive during the whole time of the experiment. Below 450 K, the concentration of atomic oxygen on defects and terraces is constant. At 450–550 K, the rate of desorption from defects $R_{II, II}$ and mixed sites $R_{I, II}$ starts to grow. As temperature increases to 600 K, the concentration of nitrogen on defects decreases to zero (Fig. 7c), and the contribution from $R_{I, II}$ to the overall desorption rate *R* increases. The migration of nitrogen atoms from terraces to defects (steps (IV)) does not result in filling defects with nitrogen atoms despite the growth of its rate $R_{I \to II}$ (Fig. 7b). Rather, it only enables desorption from mixed sites. From 600 K on, the rate of desorption from terraces $R_{I, I}$ increases. Below 740 K, the contribu-

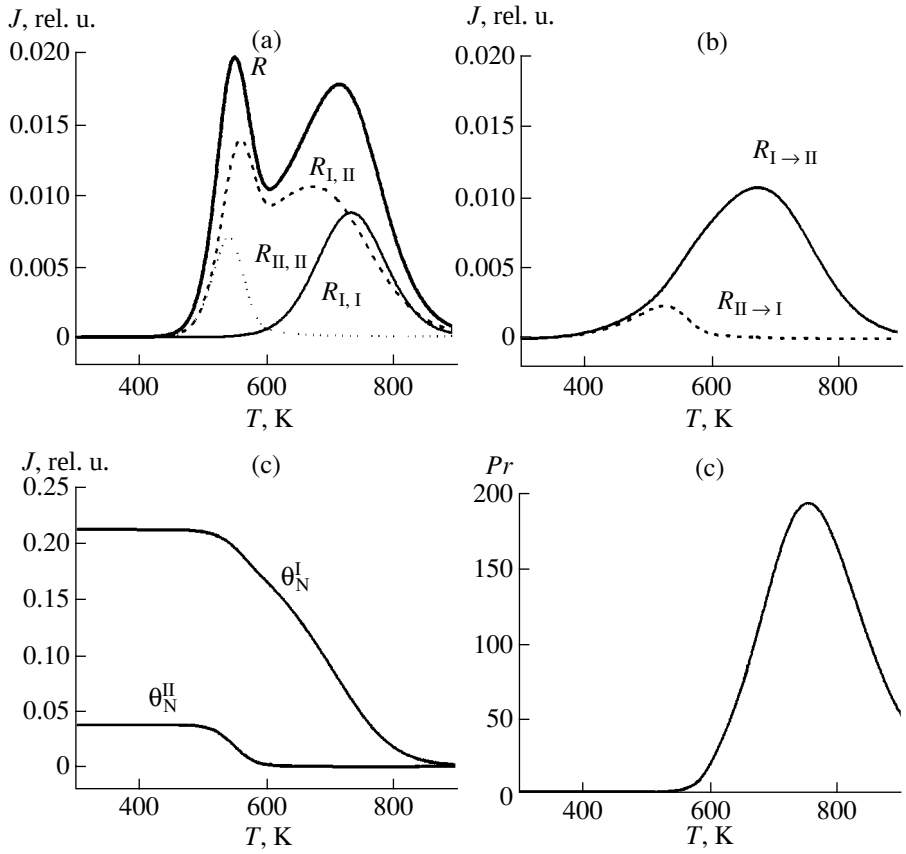

Fig. 7. The structure of the thermal desorption spectra of nitrogen (monatomic-step deterministic model) at $z = 0.15$: (a) the rate of the thermal desorption of nitrogen from defects $R_{II,II}$, terraces $R_{I,I}$, mixed sites $R_{I,II}$ and the overall rate R; (b) the rates of nitrogen in-flow from terraces onto the defects $R_{I \to II}$ and back $R_{II \to I}$; (c) changes in the concentrations of nitrogen on terraces and defects with an increase in temperature; (d) dependence of ratio of exchange rates Pr on temperature.

tion of $R_{I, II}$ to R remains dominating, but then the main contribution starts to come from $R_{I, II}$. Note that at high temperatures desorption from mixed sites is completely limited by forward reaction (IV). This is seen when one compares the dependences $R_{I, II}(T)$ and $R_{I \to II}(T)$ shown in Figs. 7a and 7b at $T > 600$ K. To characterize the proximity of the adsorbed layer to the equilibrium state, let us introduce a function $Pr(T)$, where $Pr = R_{I \to II}/R_{II \to I}$ [19]. Figure 7d illustrates the second feature of the results: during desorption, $Pr \gg 1$; that is, the equilibrium state is not settled even at a high temperature. Note that at $Pr \neq 1$, exchange steps limit the process of desorption and affect thermal desorption spectra.

Numerous experimental studies confirm that the effect of surface defects and subsurface species on the rates of elementary steps is nontrivial (see, e.g., [15]). Multiple acceleration of some processes and deceleration of others are associated with the formation of special adsorption species, which differ from species adsorbed on terraces in the structure of their electron bonds. In this work, we assume that subsurface oxygen introduced into geometrical defects favors an increase in the rate of N_2 desorption (steps (II) and (III)), but it hinders the exchange of nitrogen atoms between terraces and defects (step (IV)). To study the effect of step (IV) on the form of thermal desorption spectra, we carried out calculations for different values of the constants of determining rates $R_{I \to II}$ and $R_{II \to I}$. Figure 8a shows thermal desorption spectra for $z = 0.15$ assuming that there is no exchange. The thermal desorption spectrum shows two pronounced maxima and a deep local minimum. Nitrogen first desorbs from defect and mixed sites and then from terraces. With an increase in z (and, correspondingly, with an increase in the concentration of subsurface oxygen), a growth of the first local maximum is seen, while the second maximum lowers. The local minimum remains deep. Comparison with Fig. 7a shows that the addition of the terrace–defect nitrogen exchange step to the kinetic scheme result in deepening the local minimum and smoothing the transition from the low-temperature to high-temperature local maximum in the thermal desorption spectrum. On the other hand, at high rates of exchange with preexponential factors $k^0_{4+} = k^0_{4-} = 10^5$ s^{-1} (forward step (IV)) does not limit the transition of atomic oxygen to defects. The thermal desorption spectrum has only one

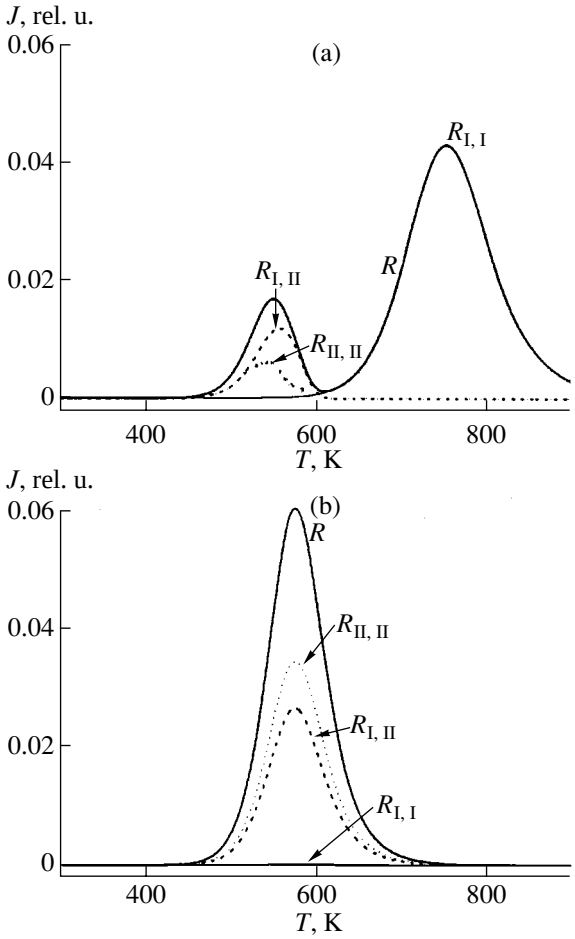

Fig. 8. Dependence of nitrogen thermal desorption (monatomic-step deterministic model) on the exchange rate at z = 0.15: (a) no exchange, $k^0_{4+} = k^0_{4-} = 0$, (b) exchange at a high rate $k^0_{4+} = k^0_{4-} = 10^5$ s^{-1}, $Pr = 1$.

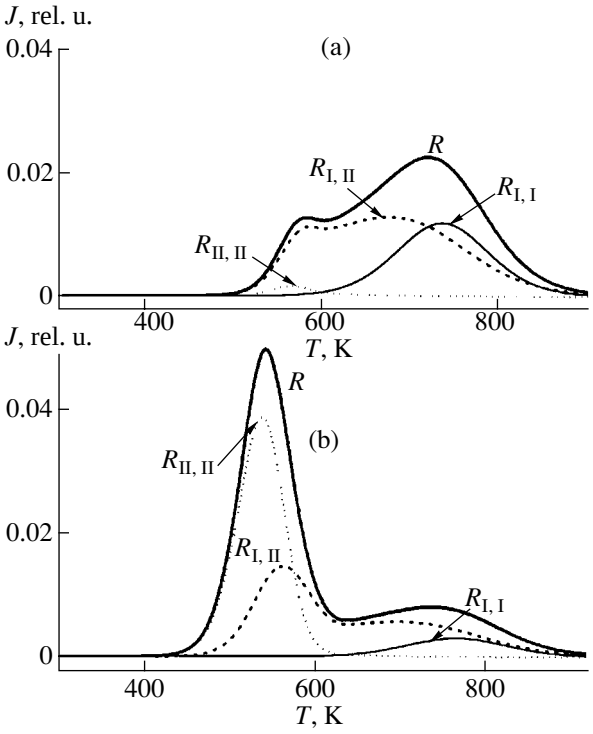

Fig. 9. Dependence of the form of thermal desorption spectrum on the initial distribution (monatomic-step deterministic model, z = 0.15): (a) all of the nitrogen is adsorbed on terraces, $\theta^{I}_{N}(t^0) = 0.25$, $\theta^{II}_{N}(t^0) = 0$; (b) all defect sites are filled with nitrogen, $\theta^{I}_{N}(t^0) = 0.1$, $\theta^{II}_{N}(t^0) = 0.15$.

low-temperature maximum in this case (Fig. 8b) corresponding to desorption from defect and mixed sites, $Pr = 1$. With an increase in the values of preexponential factors of step (IV), the structure of spectra does not change.

Results shown in Figs. 6–8 were obtained assuming that the initial distribution of nitrogen atoms over the active sites is uniform. However, at a low rate of exchange, the initial distribution of nitrogen may substantially affect the form of thermal desorption spectra. Suppose all of the nitrogen atoms are adsorbed on terraces at the initial moment; that is, $\theta^{I}_{N}(t^0) = \theta_N(t^0) = 0.25$ and $\theta^{II}_{N}(t^0) = 0$. The corresponding thermal desorption spectrum is shown in Fig. 9a. Because the rates of exchange are low, nitrogen atoms largely remain adsorbed on terraces. Below 700 K, desorption largely occurs from the mixed sites, and the contribution of desorption from defect sites is insignificant. This results in a shift of the position of the low-temperature maximum compared to Fig. 7 to the region of high temperatures ($T_1 \approx 570$ K) and in a decrease in its intensity. The local minimum preserves its position, and an increase in its intensity is explained by the higher concentration of nitrogen on terraces. Figure 9b illustrates the opposite case. At the initial moment, nitrogen covers all defects. In this case, the thermal desorption spectrum has a pronounced low-temperature maximum, which describes the intensive desorption from defect and mixed sites, and a weak high-temperature maximum. Note that, in the last example, the assumption of the nonuniform initial distribution of nitrogen over the surface characterized by the predominant filling of defects has numerous experimental confirmations [15].

Experimental studies were carried out at a rather high rate of heating of the sample (up to 40 K/s). By decreasing the heating rate at any constant nonzero rate of exchange (specifically, at the values of parameters of Fig. 7), one may theoretically obtain the thermal desorption spectrum with the single low-temperature maximum. For instance, for b = 2 K/s, step (IV) does not limit desorption from defects, and the recombination of atomic nitrogen occurs at a low temperature unlike in the case of Fig. 7.

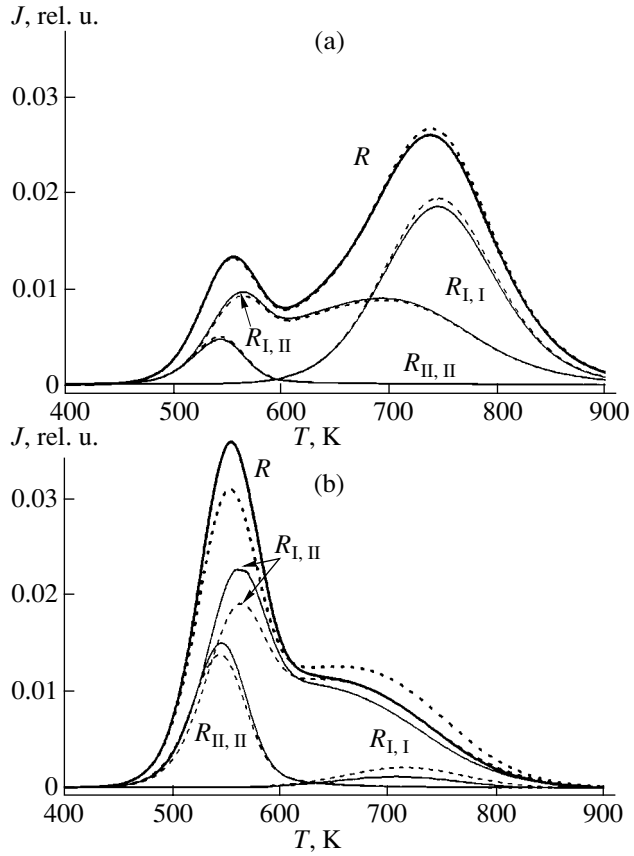

Fig. 10. Comparison of the thermal desorption spectrum of nitrogen calculated using the deterministic models: the monatomic-step model (solid line) and the chain-armor model (dashed line) for different values of z: (a) 0.1 and (b) 0.25.

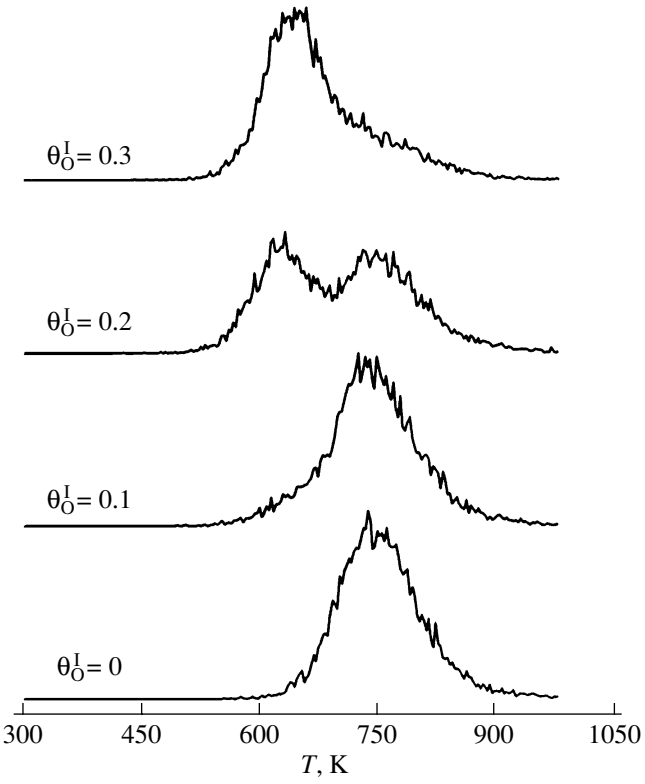

Fig. 11. Thermal desorption spectra of N_2 from Ir(111) (the L_{tr} model) for different values of θ_O^I. $\varepsilon_{NN}^1 = \varepsilon_{NO}^1 = \varepsilon_{OO}^1 =$ –1.6 kcal/mol, $\varepsilon_{NN}^2 = \varepsilon_{NO}^2 = \varepsilon_{OO}^2 = 0.8$ kcal/mol, $\theta_N^I(t^0) = 0.25$; stochastic model; averaging over 10 realizations.

Finally, let us clarify the role of desorption from mixed sites (step (III)). In the above results, we assumed that $k_3^0 = 0.5k_2^0$ and $E_3 = E_2$. This means that a subsurface oxygen atom influences a larger surface area than only the active site above it. The calculation showed that a decrease in the preexponential factor of the rate of nitrogen desorption from mixed sites k_3^0 or the absence of this step does not qualitatively affect the overall thermal desorption spectra, although it does change their structure. For the low-temperature desorption channel of equal intensity, the higher density of geometric defects is needed.

The chain-armor model (4), (6). As we expected, the results of calculations according to the deterministic chain-armor model are close to the results obtained using the monatomic-step model. Figure 10 compares the thermal desorption spectra of nitrogen calculated using the monatomic-step and chain-armor models for two values of z. At $z = 0.1$, thermal desorption spectra are the same according to both models, whereas at $z = 0.25$ they differ insignificantly: the chain-armor model gives the less intensive low-temperature maximum and the more flat high-temperature shoulder.

Stochastic model. The goal of Monte Carlo modeling in this work was to study the effect of lateral interactions in the adsorbed layer on the thermal recombination of atomic nitrogen on geometrically uniform surfaces and on surfaces with structural defects.

The model of closed-packed Ir(111) face L_{tr}. It is well known that the assumption of lateral interactions in the adsorbed layer on the thermal recombination of atomic nitrogen on geometrically uniform surface may introduce qualitative changes to the dependences of the average characteristics of the reaction system on external parameters and time obtained in the framework of the ideal model [12, 13]. Specifically, additional local maxima and flat regions may appear in thermal desorption spectra stipulated by the formation and destruction of the fragment of the ordered phase in the adsorbed layer.

The study of an alternative mechanism for the appearance of the low-temperature channel of N_2 thermal desorption from Ir(111) based on the consideration of paired additive lateral interactions of adsorbed spe-

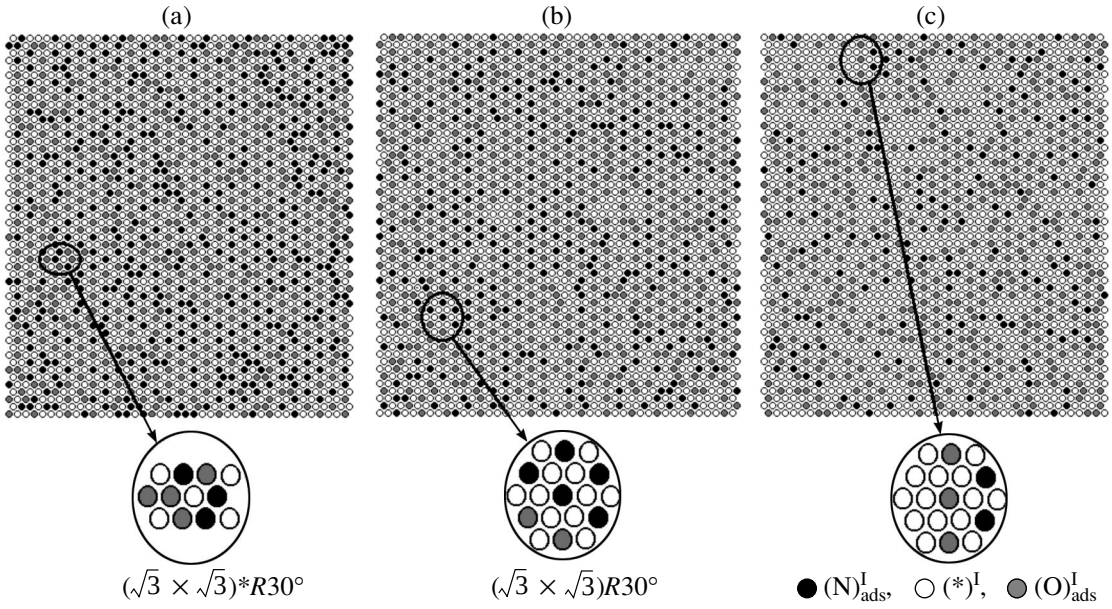

Fig. 12. Instant images of the microstate of the L_{tr} lattice fragment; $\theta^I_N(t^0) = 0.25$, $\theta^I_O = 0.2$; (a) $T = 620$ K, $\theta^I_N = 0.217$; (b) $T = 690$ K, $\theta^I_N = 0.136$; (c) $T = 750$ K, $\theta^I_N = 0.079$.

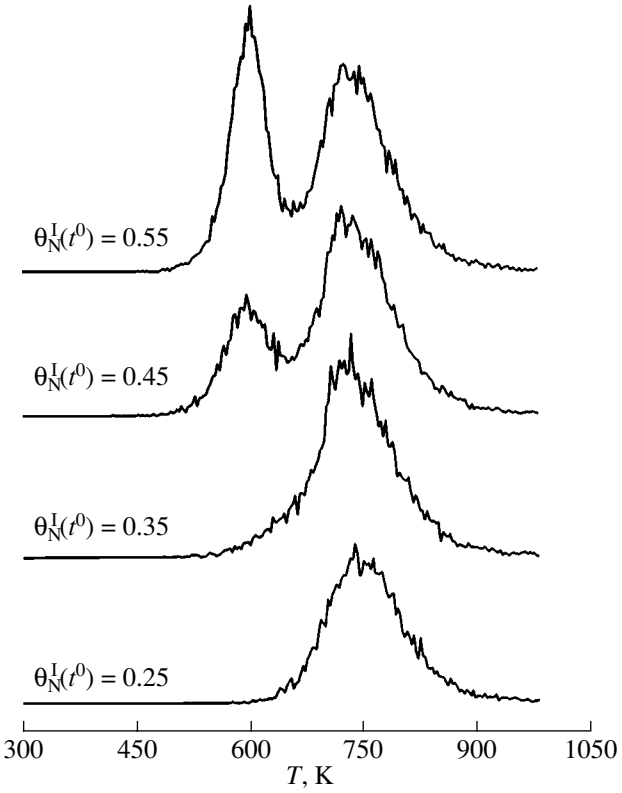

Fig. 13. Results of stochastic modeling of the thermal desorption of N_2 from Ir(111) (the L_{tr} model) for different initial concentrations $\theta^I_N(t^0)$. $\theta^I_O = 0$, $\varepsilon^1_{NN} = -1.6$ kcal/mol, $\varepsilon^2_{NN} = 0.8$ kcal/mol.

cies at next-nearest-neighbor distances according to the reduced kinetic scheme (I), (V), (VI) was carried out using a fragment of triangulated lattice L_{tr} consisting of 8100 nodes ($N_1 = N_2 = 90$) with periodic boundary conditions.

The calculation showed that the best description of experimental thermal desorption spectra of nitrogen is achieved using the assumption that the fragments of ordered phase are formed in the adsorbed layer when some specific rate constants of adsorbed species migration are chosen. These fragments have a mixed composition and contain nitrogen and oxygen atoms. The values of parameters characterizing lateral interactions are shown in Table 2 (variant 1).

In contrast to the thermal desorption spectrum of the ideal adsorbed layer (Fig. 6a), in the case of the nearest-neighbor repulsion of nitrogen and oxygen atoms ($\varepsilon^1_{NN} = \varepsilon^1_{NO} = \varepsilon^1_{OO} = -1.6$ kcal/mol) and weak next-nearest-neighbor attraction ($\varepsilon^2_{NN} = \varepsilon^2_{NO} = \varepsilon^2_{OO} = 0.8$ kcal/mol) on the geometrically uniform surface, an additional low-temperature channel of N_2 desorption may appear (Fig. 11). The energy of paired nearest-neighbor (second) interactions of adsorbed species A and B is denoted by ε^1_{AB} (ε^2_{AB}). The "minus" sign stands for repulsion. The appearance of the low-temperature local minimum in the thermal desorption spectrum is associated in this case with the formation of the mixed ordered phase in the adsorbed layer. For the chosen values of energy parameters of paired interactions, the coverage with the following structures can be formed

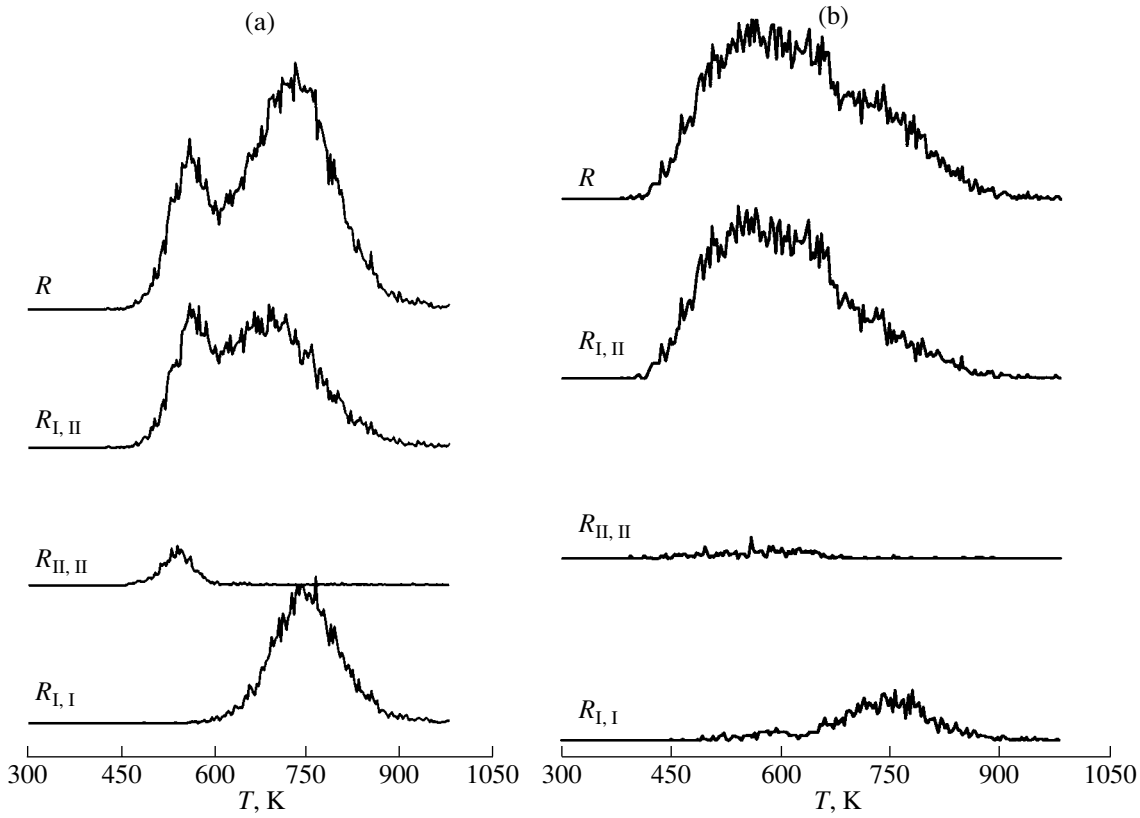

Fig. 14. Results of stochastic modeling of the thermal desorption of N_2 from the polycrystalline iridium surface (the L^*_{tr} (0.1) model), $\theta^I_N(t^0) = 0.225$, $\theta^{II}_N(t^0) = 0.025$, $\theta^I_O = 0.2$; (a) no lateral interactions, (b) $\varepsilon^1_{NN} = \varepsilon^1_{NO} = \varepsilon^1_{OO} = -1.6$ kcal/mol, $\varepsilon^2_{NN} = \varepsilon^2_{NO} = \varepsilon^2_{OO} = 0.8$ kcal/mol.

on the surface depending on the overall concentration of adsorbed species $\theta^I(t) = \theta^I_N(t) + \theta^I_O(t)$: (a) (1×1) at $\theta^I \approx 1$ when each adsorbed species has six second neighbors, (b) $(\sqrt{3} \times \sqrt{3})^*R30°$ at $\theta^I \approx 0.66$ (six first neighbors), (c) $(\sqrt{3} \times \sqrt{3})R30°$ at $\theta^I \approx 0.33$ (six second neighbors). Otherwise the coverage may consist of different structural fragments or isolated species that do not interact with their neighborhoods [29].

Let us trace the dynamics of order/disorder transitions in the adsorbed layer using the thermal desorption spectra of nitrogen at $\theta^I_O = 0.2$ and $\theta^I_N(t^0) = 0.25$. The spectrum has three local extrema (Fig. 12). The low-temperature maximum at ≈620 K largely characterizes nitrogen desorption from the domains of the 1×1 and $(\sqrt{3} \times \sqrt{3})^*R30°$ structures (Fig. 12a). Desorption is stimulated by the nearest-neighbor repulsion. Note that for the used energy parameters and equal rates of nitrogen and oxygen atom migration, the position of the low-temperature maximum in the thermal desorption spectrum is insensitive to the concentration of adsorbed oxygen. This feature of calculated spectra agrees with experimental data. Numerical studies showed that a change in the ratio of the parameters of nitrogen and oxygen atom migration and/or the values of energy of paired interactions may result in the disappearance of the low-temperature maximum or in an increase in its sensitivity to the concentration of surface oxygen. In the latter case, the low-temperature maximum shifts toward lower temperatures with an increase θ^I_O. The local minimum at ≈690 K corresponds to the formation of close-to-ideal coverage with the $(\sqrt{3} \times \sqrt{3})R30°$ pattern (Fig. 12b). With an increase in temperature, the effect of lateral interactions on the rates of surface processes weakens. This results in the decomposition of domains with the $(\sqrt{3} \times \sqrt{3})R30°$ pattern due to desorption and migration processes (Fig. 12c). The decompositions of domains with the $(\sqrt{3} \times \sqrt{3})R30°$ pattern is described by the high-temperature part of the spectrum ($T \approx 690$ K) with a maximum at 750 K.

The appearance of the low-temperature associative adsorption on the geometrically uniform surface is observed not only in the mixed, but also in the uniform

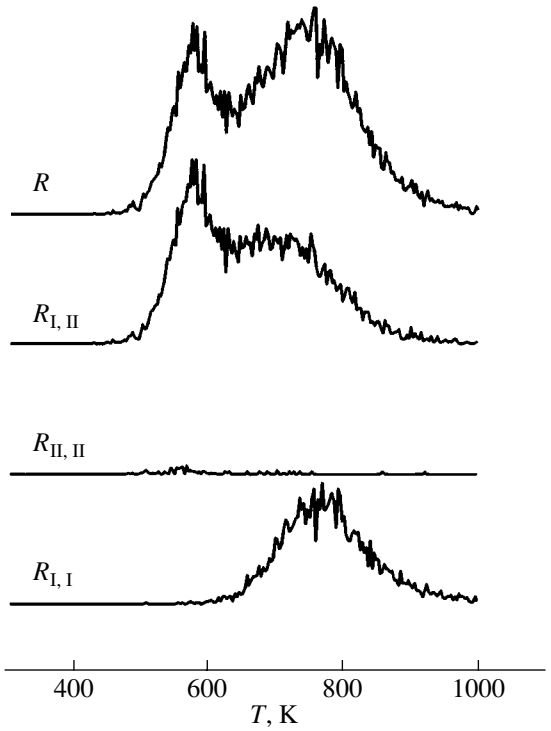

Fig. 15. Thermal desorption spectra of N_2 from Ir(110) (the L_{rec} model); $\theta_O^I = 0.2$, $z = 0.1$, $\theta_N^I(t^0) + \theta_N^{II}(t^0) = 0.25$, stochastic model 10 realizations.

adsorption layer consisting of interacting mobile species of the same type (Fig. 13; Table 2, variant 2). The intensity of the low-temperature maximum is determined by the initial concentration of adsorbed species. The addition of other species (oxygen) to the adsorbed layer do not change the thermal desorption spectra compared to Fig. 13 provided that oxygen species do not interact with the species of the first type (nitrogen). Therefore, we rejected the mechanism of low-temperature N_2 desorption that only assumes the interaction of nitrogen atoms (Table 2, variant 3) since it contradicts experimental data.

Thus, our study showed that the description of the thermal desorption of nitrogen on iridium from nonideal adsorbed layer consisting of interacting species by scheme (I), (V), (VI) conflicts with the experiment.

The monatomic-step model $L_{tr}^*(z)$. Let us first ensure that the deterministic model (4), (5) and the stochastic model of N_2 thermal desorption from the geometrically nonuniform surface of the monatomic-step type (Fig. 5b) give analogous results assuming the high rates of noninteracting species migration (steps (V)–(VII)). Let us consider a fragment of the triangular lattice $L_{tr}^*(0.1)$ ($N_1 = N_2 = 90$). Ninety percent of active sites on this lattice are on terraces and the rest are on defects with subsurface oxygen. Let us also consider the periodical boundary conditions. Figure 14a shows the thermal desorption spectra of nitrogen obtained by simulating the elementary steps (I)–(VII). The values of model parameters are summarized in Table 1. The overall spectrum *R* has pronounced low-temperature and high-temperature maxima and a local minimum agrees with the corresponding thermal desorption spectrum obtained in the framework of the deterministic model (4), (5) and shown in Fig. 6. The results of calculations according to the stochastic and deterministic models were also very close at different defect concentrations.

The assumption of lateral interactions in the adsorbed layer may substantially change the thermal desorption may patterns. Figure 14b shows the thermal desorption spectra of N_2 at $z = 0.1$ (the monatomic-step model) for the values of energy parameters of lateral interactions shown in Table 2. The local minimum and the high-temperature maximum of the thermal desorption spectrum transformed into a high-temperature shoulder under the action of surface phase transitions.

The attraction of nearest and next-nearest neighbors usually shifts the positions of maxima in thermal desorption spectra toward higher temperatures, and the intensity of the low-temperature maximum noticeably decreases. Repulsion leads to a more intensive desorption at low temperatures.

Analogous results were obtained for the chain-armor model.

The model of the rough Ir(110) L_{rec} *surface.* We assume that, in contrast to iridium foil, atomic subsurface oxygen on Ir(110) is distributed randomly. The results of numerical modeling of the thermal recombination of atomic nitrogen on the rough Ir(110) face using kinetic scheme (I)–(VII) are qualitatively analogous to the results obtained for the monatomic-step and chain-armor models of the polycrystalline surface. Figure 15 shows the structure of one of the thermal desorption spectrum of N_2 obtained using stochastic modeling. Overall, the comparative analysis of calculated thermal desorption spectra of N_2 from the Ir(110) surface and iridium foil within the framework of the generalized physicochemical model assuming the presence of subsurface oxygen supported the experimental conclusion that the surfaces have close catalytic properties with respect to the thermal desorption of nitrogen.

To conclude this section, we note the multiplicity of the joint effects of lateral interactions and the limited mobility of adsorbed species on the results of the numerical modeling of the associative desorption of nitrogen and its interaction with oxygen. One of the most interesting results of the stochastic modeling is the appearance of the high-temperature desorption maximum at the high rates of nitrogen exchange between terraces and defects due to the blocking of atomic nitrogen by immobile oxygen on terraces.

CONCLUSION

In this work we proposed and studied physicochemical and mathematical models of atomic nitrogen recombination in the presence of adsorbed oxygen on the surfaces of iridium foil and Ir(111) and Ir (110) faces.

We showed that the effect of atomic oxygen on the thermal desorption spectra of N_2 observed in the experiments can be simulated if we assume the modification of the adsorption properties of surface sites by subsurface oxygen. Oxygen penetrates into subsurface layers on rough faces and at the structural defects of the catalyst surface.

We studied the conditions for the appearance of the low-temperature associative thermal desorption from the nonideal adsorbed layer consisting of interacting species without subsurface oxygen. In this case, the qualitative agreement between experimental and simulated data is achieved with a certain choice of the species interaction parameters and the rates of migration. Therefore, the study of the mechanism for the appearance of the low-temperature channel of N_2 desorption on iridium foil and Ir(110) due to lateral interactions in the adsorbed layer is only of theoretical interest.

The joint effect of the mechanisms cited above on the form of nitrogen thermal desorption spectra is studied.

ACKNOWLEDGMENTS

We thank the Corresponding Member of the Russian Academy of Science, M.G. Slin'ko for attention to this work and useful notes and N.V. Peskov (Moscow State University) for fruitful discussions. This work was supported by the Russian Foundation for Basic Research (project no. 00-01-000587).

REFERENCES

1. Boreskov, G.K., *Geterogennyi kataliz* (Heterogeneous Catalysis), Moscow: Nauka, 1986.
2. Zhdanov, V.P., *Elementarnye fiziko-khimicheskie protsessy na poverkhnosti* (Elementary Physicochemical Processes on Surfaces), Novosibirsk: Nauka, 1988.
3. Zhdan, P.A., Boreskov, G.K., Boronin, A.I., *et al.*, *J. Catal.*, 1979, vol. 60, p. 93.
4. Boronin, A.I. and Zhdan, P.A., *Izv. Akad. Nauk SSSR, Ser. Fiz.*, 1982, vol. 46, p. 1247.
5. Gobden, P.D., Nieuwenhuys, B.E., Esch, F., *et al.*, *Surf. Sci.*, 1998, vol. 416, p. 264.
6. Kortuke, O. and von Niessen, W., *Surf. Sci.*, 1998, vol. 401, p. 185.
7. Hirsimaki, M., Suhonen, S., Pere, J., *et al.*, *Surf. Sci.*, 1998, vols. 402–404, p. 187.
8. Wang, H., Tobin, R.G., Fisher, G.B., *et al.*, *Surf. Sci.*, 1999, vol. 440, p. 429.
9. Boronin, A.I., *Cand. Sci. (Chem.) Dissertation*, Novosibirsk: Inst. of Catalysis, 1983.
10. Ibbotson, D.E., Wittrig, T.S., and Weinberg, W.H., *Surf. Sci.*, 1981, vol. 110, p. 294.
11. Myshlyavtsev, A.V. and Yablovskii, G.S., in *Mekhanizmy adsorbtsii i kataliza* (Mechanisms of Adsorption and Catalysis), Novosibirsk: Inst. of Catalysis, 1989.
12. Makeev, A.G. and Semendyaeva, N.L., *Mat. Model.*, 1995, vol. 7, no. 3, p. 29.
13. Makeev, A.G. and Slinko, M.M., *Surf. Sci.*, 1996, vol. 359, p. 467.
14. Samarskii, A.A. and Slin'ko, M.G., *Izv. Ross. Akad. Nauk, Ser. Khim.*, 1998, no. 10, p. 1895.
15. Smirnov, M.Yu. and Gorodetskii,V.V., in *Mekhanizmy adsorbtsii i kataliza* (Mechanisms of Adsorption and Catalysis), Novosibirsk: Inst. of Catalysis, 1989.
16. Cornish, J.C.L. and Avery, N.R., *Surf. Sci.*, 1990, vol. 235, p. 209.
17. Boronin, A.I. and Elokhin, V.I., *Proc. of the First Soviet–Chinese Seminar on Catalysis*, Novosibirsk, 1990.
18. Belton, D.N., DrMaggio, C.L., and Simon, K.Y., *J. Catal.*, 1993, vol. 144, p. 273.
19. Savchenko, V.I., *Kinet. Katal.*, 1994, vol. 35, no. 3, p. 349
20. Langmuir, I., *J. Am. Chem. Soc.*, 1915, vol. 37, p. 1139.
21. Redhead, P.A., *Vacuum*, 1962, vol. 12, no. 4, p. 203.
22. *Practical Surface Analysis by Auger and X-ray Photoelectron Spectroscopy*, Briggs, D. and Seah, M.P., Eds., New York: Wiley, 1983.
23. Wang, H., Tobin, R.G., Fisher, G.B., *et al.*, *Surf. Sci.*, 1999, vol. 440, p. 429.
24. *Monte Carlo Methods in Statistical Physics*, Binder, K., Ed., Berlin: Springer, 1979.
25. Eyring, H., Lin, S.H., and Lin, S.M., *Basic Chemical Kinetics*, New York: Wiley, 1980, p. 528.
26. Elenin, G.G., *Ross. Khim. Zh.*, 1996, vol. 40, no. 2, p. 19.
27. Tovbin, Yu.K., *Teoriya fiziko-khimicheskikh protsessov na granitse gaz–tverdoe telo* (Theory of Physicochemical Processes at the Gas–Solid Interface), Moscow: Nauka, 1990.
28. Gear, C.W., *Numerical Initial Value Problems in Ordinary Differential Equations*, Englewood Cliffs: Prentice-Hall, 1971, chapter 9.
29. Roberts, M.W. and McKee, C.S., *Chemistry of the Metal-Gas Interface*, Oxford: Clarendon, 1979.